Chapter 8

Amorphous, Polymorphous, and Microcrystalline Silicon Thin Films Deposited by Plasma at Low Temperatures

Mario Moreno, Roberto Ambrosio, Arturo Torres, Alfonso Torres, Pedro Rosales, Adrián Itzmoyotl and Miguel Domínguez

Additional information is available at the end of the chapter

http://dx.doi.org/10.5772/63522

Abstract

The present chapter is devoted to the study of amorphous (a-Si:H), polymorphous (pm-Si:H), and microcrystalline (μc-Si:H) silicon, deposited by the plasma-enhanced chemical vapor deposition (PECVD) technique at low temperatures. We have studied the main deposition parameters that have strong influence on the optical, electrical, and structural properties of the polymorphous and microcrystalline materials. Our results reveal the key deposition conditions for obtained films with optical and electrical characteristics, which are suitable for applications on thin-film solar cells and semiconductor devices.

Keywords: amorphous, polymorphous, microcrystalline, silicon, nanocrystals

1. Introduction

At the present time hydrogenated amorphous silicon (a-Si:H) is a mature material of the microelectronics and photovoltaic industries. Its success is due to the compatibility with the silicon CMOS technology, the possibility of doping (n or p type), the low substrate temperatures used (≤300°C) when is deposited by the plasma-enhanced chemical vapor deposition (PECVD) technique, and the possibility to deposit it over very large substrate areas (>1 m^2), such

as glass, metal foils, or plastic flexible substrates. Thin-film transistors (TFTs), large-area thin-film solar cells, and high-performance infrared (IR) cameras (based on microbolometer arrays) among others are devices based on the a-Si:H technology.

However, despite the important characteristics of a-Si:H, it has several drawbacks, such as a large density of defects, poor transport properties such as low carriers' mobility, and poor stability against radiation [1, 2], which limits its applications in new and high-performance devices. In this aspect, there exists a constant study of the optimization of the deposition conditions of a-Si:H films by the PECVD technique, in order to improve its performance characteristics and to produce other materials with different structural, electrical, and optical characteristics.

Recently, it has been demonstrated that it is possible to produce nanocrystals, of about 3–5 nm of diameter, in the a-Si:H matrix, by modifying the deposition conditions of standard a-Si:H, using the PECVD technique. The above material is commonly referred as polymorphous silicon (pm-Si:H) [3–6]; the presence of nanocrystals distributed on the silicon amorphous matrix reduces the density of states (DOS) and defects and improves the electrical properties, as carriers' mobility and stability of the films against radiation [3–6]. Moreover, pm-Si:H also preserves the characteristics of a-Si:H as a direct band gap, high absorption coefficient, and high activation energy (E_a).

Therefore pm-Si:H films can replace a-Si:H in devices as the intrinsic film in a-Si:H thin-film solar cells. It has been reported that a-Si:H thin-film solar cells suffer from degradation due to constant illumination (Staebler-Wronski effect, SWE [7]); therefore the initial solar cell efficiency is reduced. As well it has been demonstrated that the use of pm-Si:H instead of a-Si:H reduces the light-induced degradation [8].

On the other hand, also by modifying the silicon film deposition conditions using PECVD, it is possible to increase the crystal sizes and the crystalline fraction of the silicon films and therefore modifying not just the film structure but also the electro-optical characteristics, as the absorption coefficient, the room temperature conductivity, the band gap, and E_a. Micro-crystalline silicon (μc-Si:H) is a silicon film where the sizes of the silicon crystals are much more larger than in pm-Si:H films, with sizes in the order of dozens of nanometers, and the overall crystalline fraction (X_C) is large, and the electro-optical characteristics are different than its a-Si:H/pm-Si:H counterpart.

The μc-Si:H thin films are suitable for various devices, such as TFTs, due their larger room temperature conductivity and carrier mobility (compared to those of a-Si:H or pm-Si:H), which are transduced in faster devices, as well the band gap and absorption coefficient are different than those of a-Si:H, resulting in thin solar cells with larger IR absorption and more stable against sun radiation. At the present time a-Si:H/μc-Si:H tandem solar cells (or also known as micromorph solar cells) have been developed with stabilized efficiencies of about 12% [9].

http://dx.doi.org/10.5772/63522

2. Plasma deposition

The a-Si:H films used in the industry are typically obtained by means of PECVD. The first work on the deposition of a-Si:H material by silane glow discharge started in 1960s [10].

The standard PECVD system consists of a reactor of two parallel electrodes capacitively coupled, separated at some distance. The substrate is placed in one of these electrodes, as is shown in **Figure 1**. The most common RF is 13.56 MHz. In the PECVD reactor, silane (SiH_4), often diluted with other precursor gases (H_2, Ar, etc.), is pumped at a certain flow rate. A substrate for the film deposition is collocated in the chamber in the bottom electrode, and a RF oscillating voltage is applied to the upper electrode of the chamber. Most of the surface chemistry occurs due to the high-energy electron bombardment. The deposition process of silicon-based films can be described as a main four-step process:

1. The primary reaction is made by the glow discharge, which results in electron-impact excitation, dissociation, and ionization of the molecules. The plasma thus consists of neutral radicals and molecules, positive and negative ions, and electrons.

2. Reactive neutral species are transported to the substrate by diffusion, positive ions bombard the growing film, and negative ions are trapped within the sheaths and may eventually form small particles.

3. The third step consists of surface reactions, such as hydrogen abstraction, radical diffusion, and chemical bonding. Then the formation of islands is made and it continues until there is a thin film.

4. The fourth step is the subsurface release of hydrogen molecules from the film.

The deposition process involved physical and chemical interactions in the plasma and at the growing film surface is dependent on several parameters such as RF power, frequency, substrate temperature, gas pressure, and electrode geometry; a deeper explanation could be found in [11].

Generally a plasma deposition system consists of several subsystems, each providing different functions. The reactor system is the central part where the molecules are dissociated and the products are deposited on heated substrates in order to form a layer. The reactor has a capacitor electrode configuration. The power to the reactor system is delivered by means of the RF source connected via the matching network. The RF source generally operates at a frequency of 13.56 MHz. The power and ground are connected to the top and bottom electrodes, respectively. The samples are loaded in the bottom electrode, which can be heated from room temperature to about 300°C. The gas control system includes mass flow controllers to measure and control the different gases (GeH_4, SiH_4, NH_3, Argon, H_2, PH_3, B_2H_3) supplied to the chamber. The vacuum system comprises mechanical pump, turbo molecular pump, roots pump, and the pressure controller system. The deposition pressure can be controlled in a wide range of values, usually from 500 to 2000 mTorr.

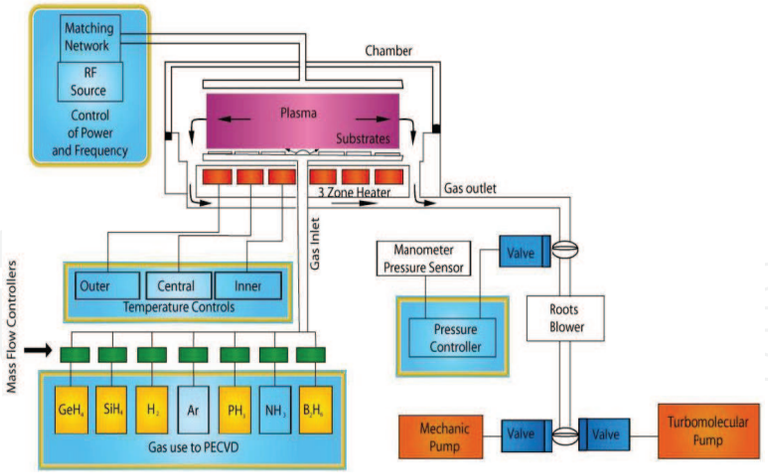

Figure 1. Scheme of a plasma deposition system (PECVD) used for film deposition. Also the power, frequency, temperature, gas flow, and pressure controls are shown.

In our particular facilities, we use a four-chamber cluster tool from MVSystems for the deposition of a-Si:H and related materials. To minimize cross-contamination between the chambers, it has a chamber for the deposition of intrinsic a-Si:H films, two chambers for the deposition of p- and n-doped semiconductor films, and a chamber for the deposition of metals and transparent conductive oxides, as is shown in **Figure 2**. The chambers are kept under high vacuum (10^{-6} torr) by turbo molecular pumps. The cluster tools eliminate cross-contamination in multilayer thin-film structures and allow the production of high-quality electronic devices [12].

Currently, several deposition techniques have been reported for the deposition of a-Si:H and nano- and microcrystalline materials, such as radio-frequency (13.56 MHz) capacitively coupled PECVD (RF-PECVD) [11], very high-frequency PECVD (VHF-PECVD) [13], microwave CVD (MW-CVD) [14], electron cyclotron resonance CVD (ECR-CVD) [15], reactive magnetron sputtering (RMS) [16], hot-wire CVD (HW-CVD) [17], and the remote expanding thermal plasma (ETP) [18].

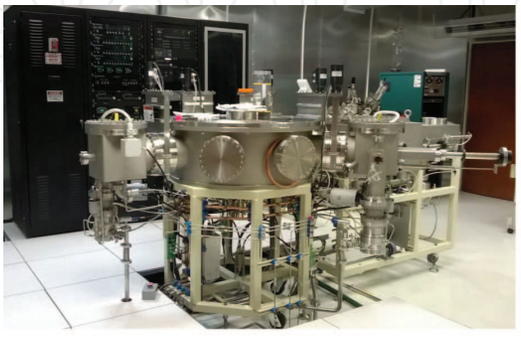

Figure 2. PECVD cluster tool from MVSystems, at the facilities of the Laboratory of Microelectronics of INAOE (project no. 152224 of the Secretary of Energy, SENER and the National Council of Science and Technology, CONACYT, Mexico).

http://dx.doi.org/10.5772/63522

One of the drawbacks for RF-PECVD at 13.56 MHz is the deposition rate, which is in the range of 1–3 Å/s. However, some efforts of increasing the RF-PECVD growth rate using higher power and pressure have been reported in [19]. The best deposition rates using the VHF in the range from 30 to 300 MHz have been reported until 20 Å/s [20].

3. Amorphous silicon

The noncrystalline semiconductors materials also known as "amorphous semiconductors" are usually obtained by the dissociation of gas species using the PECVD technique [21, 22]. In these materials the chemical bonding of atoms is a random covalent network; the disorder variation in the angles between bonds eliminates the regular lattice structure of its crystalline counterpart, as is shown in **Figure 3**. However, the noncrystalline semiconductors have demonstrated good optical and electronic properties for many device applications.

Hydrogenated a-Si:H is a mature material in the electronics manufacturing industry, where it is used for the development of thin-film solar cells, IR sensors, and TFTs, due to its very large absorption coefficient, its compatibility with the standard Si-CMOS technology, and the low process temperatures used (<300°C) when it is deposited by PECVD. The above features allow the use of different substrates such as metal foils, plastics, and glasses. In **Table 1** a comparison of Si-CMOS technology in contrast to the TFT technologies is shown. From the point of view of the process temperature and cost, a-Si:H technology is very attractive for flexible and low-cost electronics.

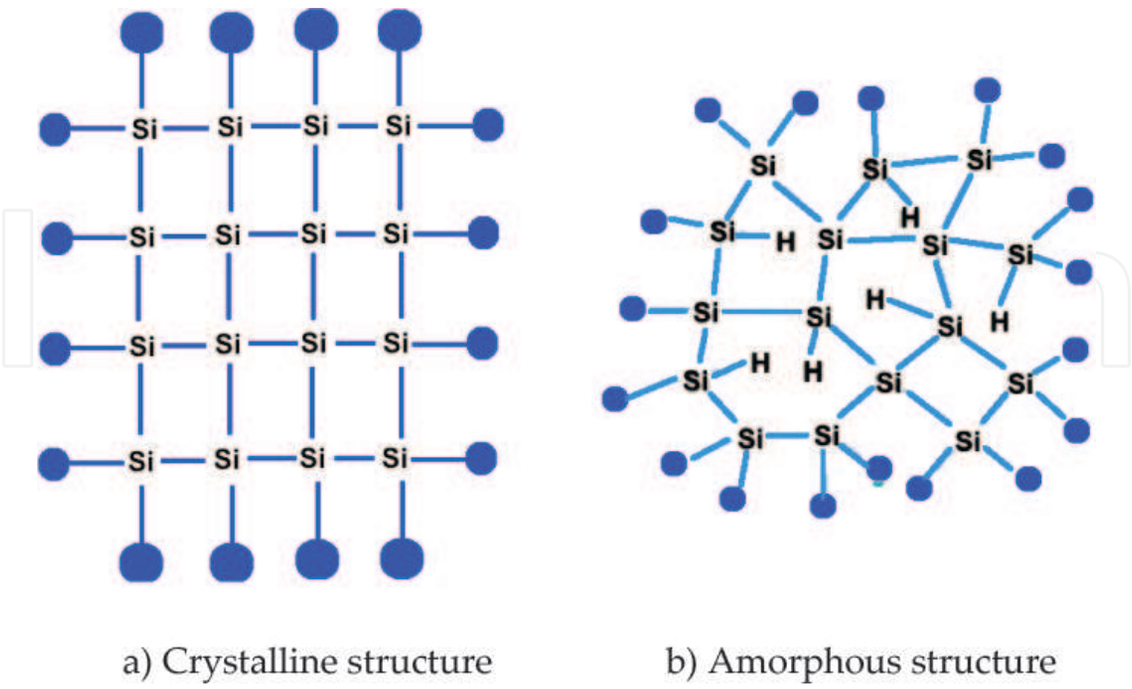

Figure 3. Schematic representation for the structures of (a) crystalline silicon (c-Si) and (b) amorphous silicon (a-Si:H).

The a-Si:H film is composed by covalent bonds of Si—Si and Si—H. The silicon atoms form covalent bonds mainly with three neighboring silicon atoms with a hydrogen atom [23]. The hydrogen contents in a-Si:H have been reported from 4% up to 40%, and the density of hydrogen atoms depends on deposition conditions. The amorphous structure of the material leads to open network structures, in which voids and un-terminated bonds are so-called defects or dangling bonds. For integration of a-Si:H into electronic devices, the defect density must be in the range from 10^{15} to 10^{16} cm^{-3} [24]. In pure a-Si, the defect density is higher (10^{19} to 10^{20} cm^{-3}) than in hydrogenated a-Si:H, which is not suitable for electronic device applications. In a-Si:H the hydrogen is responsible for the lowering of the defect density by passivation of these dangling bonds [25]. This is crucial because of the influence of the optoelectronic properties, since in a-Si:H the dangling bonds can act as efficient recombination centers for electrons and holes. The increase in defect density with light radiation (light soaking) is the main cause of the SWE [26], where the light induces a creation of metastable defects in a-Si:H. These additional dangling bonds can be reduced by heating the sample up to approximately 200°C. Some works have reported the reduction of that effect by incorporating fluorine in the gas mixture during production [27].

Parameter Technology	**Device technology**		
	c-Si MOSFET	**a-Si:H TFT**	**Organic TFT**
Process temperature	1000°C	200°C	<100°C
Process technology	Photolithography multilayers	Photolithography multilayers	Shadow mask and ink-jet
Design rule	<32 nm	8 μm	50 μm
Substrate	Wafer	Glass/plastic	Plastic/metal foil
Supply voltage	1 V	20 V	Ink-jet 40 V
Device type	N-type and P-type	N-type	P-type
Mobility	1500 cm^2/Vs	1 cm^2/Vs	0.5 cm^2/Vs
Cost/area	High	Medium	Low
Lifetime	Very high	High	Medium–low

Table 1. Comparison of TFT and CMOS technology [23].

In amorphous semiconductors, the disorder and the presence of dangling bonds have an influence on the electronic DOS. **Figure 4** shows a simple schematic diagram of the DOS of the conduction band (delocalized states) and the valence band (delocalized states) from the Davis-Mott model, where E_c and E_v represent the energies, which separate the ranges where the states are localized and extended. The central band is split into a donor and an acceptor band.

In the above model, the mobility has a drop in several orders of magnitude at the transition from extended to localized states, resulting on a mobility edge. Thus the interval between E_c and E_v acts as a pseudo-gap (referred as the mobility gap) [28].

http://dx.doi.org/10.5772/63522

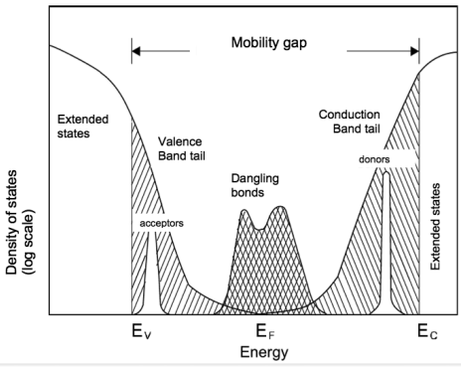

Figure 4. Schematic representation of DOS based on Davis-Mott model [28].

There are several definitions for optical gap and conventionally Tauc optical gap is used among others. Thus, the band gap can be approximated using the measurements of the optical absorption coefficient.

$$\alpha(h\nu)=(A/h\nu)(h\nu-E_T)^2 \quad (1)$$

where h is Planck's constant, α is the absorption coefficient, ν is the radiation frequency, E_T is the optical band gap, and A is a proportional constant.

The absorption coefficient of a-Si:H is showed in **Figure 5**, where three main regions in the spectra are typical identified, which are due to (a) band-to-band transitions that correspond to the transitions from valence to conduction band, (b) transitions related to valence and conduction band tails, and (c) defect-related transitions.

Figure 6 shows a HRTEM cross-sectional view of an a-Si:H thin film deposited in our facilities; in the figure it is observed that there is not a larger range order of the atoms in the material, which is the main structural characteristic of amorphous semiconductors.

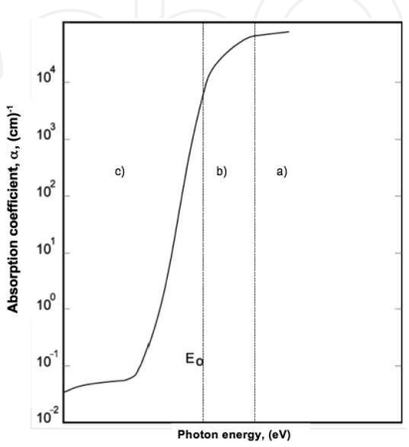

Figure 5. Typical absorption coefficient of a-Si:H plotted as a function of photon energy [28].

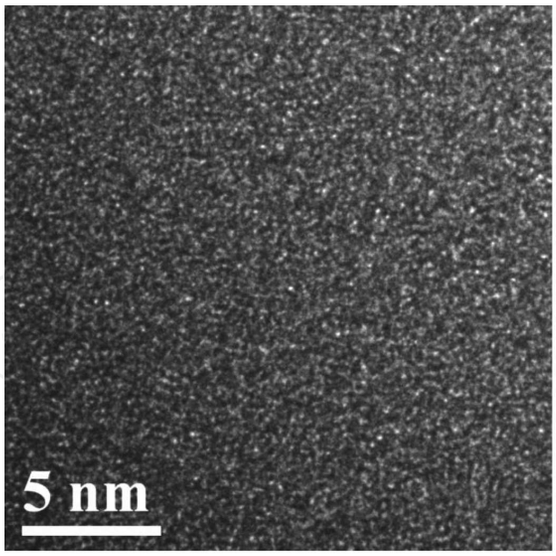

Figure 6. Cross section of an a-Si:H thin film observed by HRTEM.

4. Polymorphous silicon (pm-Si:H)

Basically pm-Si:H is a-Si:H with embedded nanocrystals of about 3–5 nm of diameter; those nanocrystals are distributed in the a-Si:H matrix. The pm-Si:H films are obtained by modifying the deposition conditions of standard a-Si:H, using the PECVD technique. The presence of nanocrystals on the silicon amorphous matrix reduces the DOS and defects and improves the electrical properties, as the carriers' mobility and the stability of the films against radiation [3–6]. Also, pm-Si:H preserves the characteristics of a-Si:H as a direct band gap, high absorption coefficient, and high activation energy (E_a). Intrinsic pm-Si:H has a direct optical band gap (1.6–1.8 eV) and a very large activation energy ($E_a \approx 1$ eV), when it is deposited by PECVD.

The above properties of pm-Si:H make this material very suitable for more stable devices as thin-film solar cells and thermal detectors. In this aspect, recently it has been reported thin-film solar cells where the a-Si:H intrinsic film has been replaced with a pm-Si:H film, resulting on solar cells with higher stability against light radiation (light soaking), in comparison with its counterpart employing a-Si:H [8].

4.1. Deposition conditions of pm-Si:H

We have performed a study of the deposition conditions of pm-Si:H by PECVD [21]. The deposition parameters were varied in order to observe their effect on the structural, electric, and optical characteristics of the films deposited. A series of pm-Si:H thin films was deposited by PECVD at RF = 13.56 MHz, from a SiH_4 and H_2 mixture. **Table 2** shows the deposition conditions for the pm-Si:H thin films; those films were deposited for 30 min, at substrate temperature T_s = 200°C. For the pm-Si:H film deposition, a high H_2 dilution is used and the chamber pressure was varied, since it is an important parameter for the production of

http://dx.doi.org/10.5772/63522

nanocrystals. Notice that here we present some selected processes, which are more representatives.

Sample #	Press. (mTorr)	Power (W)	Power density (mW/cm^2)	SiH_4 flow (sccm)	H_2 flow (sccm)
P1	500	20	69	50	50
P2	1000	20	69	50	50
P3	1500	20	69	50	50

Table 2. Deposition conditions of pm-Si:H films.

4.2. Characterization of pm-Si:H

4.2.1. Deposition rate

The deposition rate (V_d) of the pm-Si:H films was calculated from the average thickness and the deposition time; in this case all the films were deposited for 30 min. **Figure 7** shows the variation of deposition rate of the pm-Si:H films as a function of deposition pressure, maintaining constant the other process parameters (see **Table 1**). In **Figure 7**, it is seen that deposition rate of the pm-Si:H films increases from 0.5 Å/s to 2.4 Å/s as the deposition pressure increases. For the pressure of 0.5 torr, the deposition rate of the film is 0.5 Å/s (which is a pressure generally used for the deposition of a-Si:H). At a pressure of 1.5 torr, the deposition rate increases to about 2.4 Å/s.

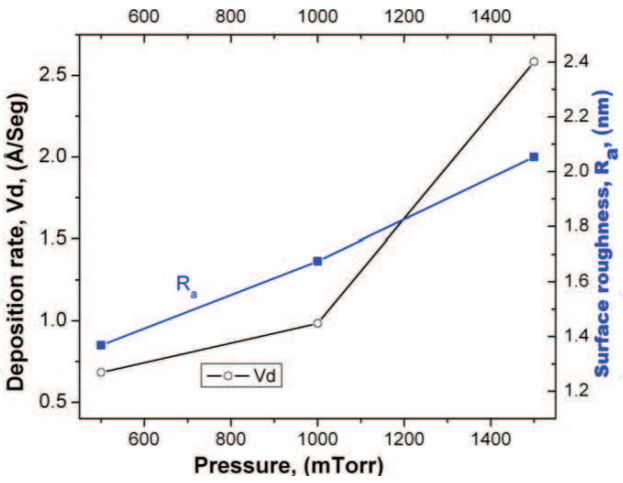

Figure 7. Deposition rate and surface roughness of pm-Si:H films as a function of the deposition pressure.

4.2.2. Structural analysis

Figure 8(a)–(c) shows three-dimensional (3D) AFM surface images of the pm-Si:H films deposited on silicon substrates; those films were deposited at different pressure values: 500, 1000, and 1500 mTorr. In the figure it is observed that the film deposited at 1500 mTorr has the

largest R_a (of about 2.05 nm), which is in agreement with the deposition rate V_d results, since larger V_d and larger roughness are associated with larger crystallinity fraction in the films. The dependence with the deposition pressure of the average surface roughness (R_a) is shown in **Figure 7** and those values are listed in **Table 3**.

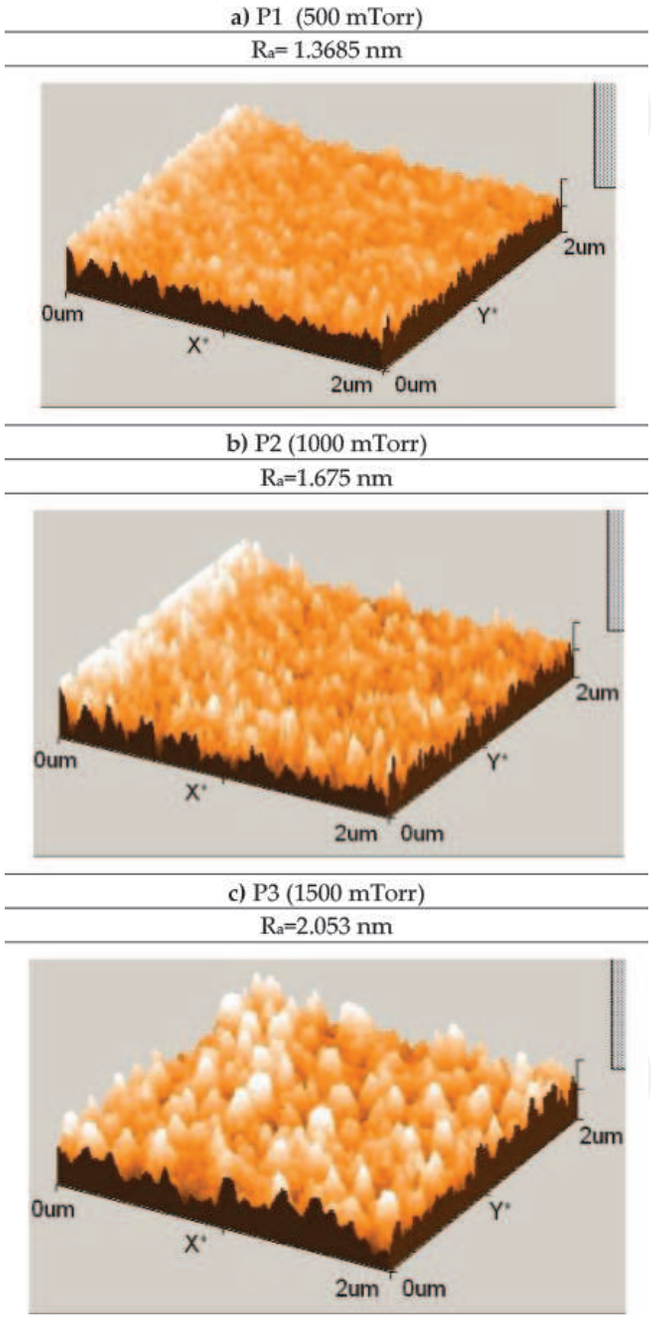

Figure 8. AFM 3D images of pm-Si:H films as a function of the deposition pressure: (a) P1 (500 mTorr); R_a = 1.3685 nm. (b) P2 (1000 mTorr); R_a = 1.675 nm. (c) P3 (1500 mTorr); R_a = 2.053 nm.

High-resolution transmission electron microscopy (HRTEM) was used to study the film's bulk transversal structure. **Figure 9** shows a transversal view of a 100 nm thick pm-Si:H film

http://dx.doi.org/10.5772/63522

deposited over (1 0 0) c-Si obtained in our previous work [22]; in the figure several nanocrystals of sizes of around (3–5 nm) are marked; it also is possible to observe the presence of nano-islands at the c-Si/pm-Si:H interface.

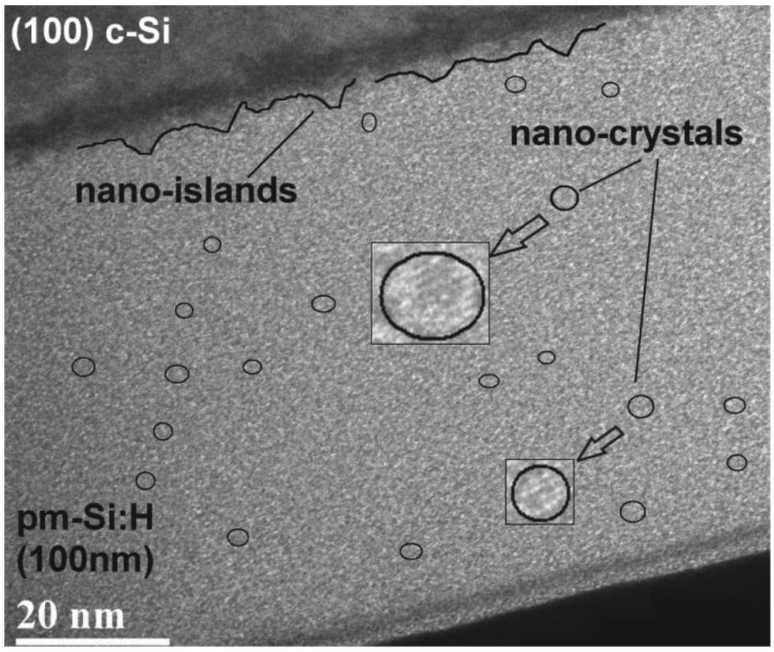

Figure 9. HRTEM image of the transversal view of a pm-Si:H film deposited by PECVD [22].

Sample #	R_a (nm)	C_H (%)	$X_{C\_(Raman)}$ (%)
P1	1.36	2.3	No sensitivity
P2	1.67	9.9	No sensitivity
P3	2.05	15.9	No sensitivity

Table 3. Surface roughness (R_a), H_2 content, and crystalline volume fraction for the pm-Si:H films.

4.2.3. Fourier transform infrared spectroscopy (FTIR) analysis

The IR absorbance spectra of the pm-Si:H thin films in the range 500–2200 cm^{-1} are shown in **Figure 10**. In the spectra several peaks related to different vibration modes are found. The peak at around 640 cm^{-1} corresponds to Si—H rocking/waging modes [29], the band at around 800–950 cm^{-1} is related to SiH_2 or SiH_3 bonding with low intensity, and it depends on deposition conditions [29–31]. The band at 1900–2100 cm^{-1} is related to SiH, SiH_2, and SiH_3 stretching modes.

In **Figure 10**, it is observed that as the pressure deposition increases, a change in the shape and intensity of the band at 640 cm^{-1} is observed. For samples, P1, P2, and P3, the total H_2 bonded

content C_H of the films was calculated with the integration of the area under the Si—H mode (at 640 cm^{-1}) using Eq. (2) [29]:

$$C_H(\%) = \frac{A_\omega}{N_{Si}} \int \frac{\alpha(\omega)}{\omega} d\omega \quad (2)$$

where α is the absorption coefficient at frequency (ω), A_ω is the oscillator strength ($A_{(640)} = 1.6 \times 10^{19}$ cm^{-2}) [29, 32], and $N_{Si} = 5 \times 10^{22}$ cm^{-3} is the atomic density of pure silicon. The IR spectrum was deconvoluted using Gaussian peaks centered for the region of interest. **Table 3** shows the H_2 content results and is observed that H_2 increases as the pressure increases. Also in **Figure 10** a shift from 700 cm^{-1} to 640 cm^{-1} from the film deposited at lower pressure to the film deposited at higher pressure is observed, which could be related to the evolution of hydrogen content on the films, and associated to the presence of nanocrystals in the films deposited at higher pressure [33]. At higher pressures there is a change in the discharge regime, which results in the formation of silicon nanocrystals (up to 2 nm), during the growth of pm-Si:H films [34, 35], and that is in agreement with the values of R_a in our AFM analysis.

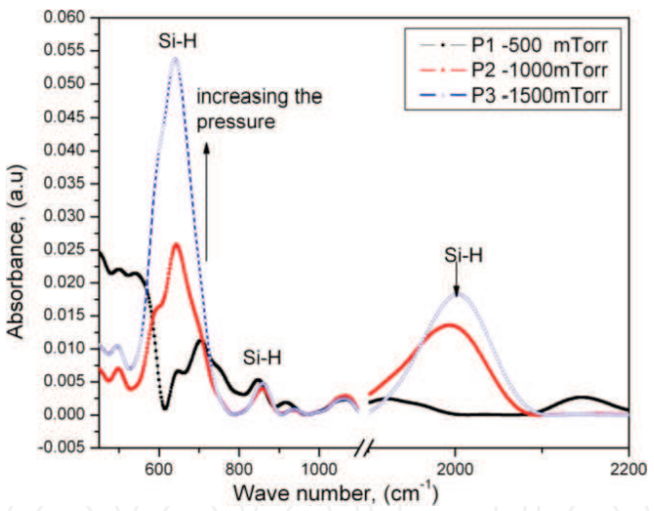

Figure 10. FTIR spectra of the pm-Si:H thin films.

4.2.4. Raman analysis

Raman-scattering measurements were performed in the pm-Si:H films. Raman spectra were deconvoluted into three bands related to an amorphous phase (480 cm^{-1}), an intermediate phase associated with small-size nanocrystals (500–514 cm^{-1}), and a crystalline phase (520 cm^{-1}). **Figure 11** shows the Raman spectra of the pm-Si:H film series.

The Raman spectra of the pm-Si:H films have a main peak located at 479 cm^{-1} (corresponding to a transverse optical phonon), which is related to an amorphous phase, and there was not

http://dx.doi.org/10.5772/63522

detected any phase related to a crystalline fraction (520 cm^{-1}). The contribution of the nanocrystals in pm-Si:H films is too small in order to be detected by Raman scattering.

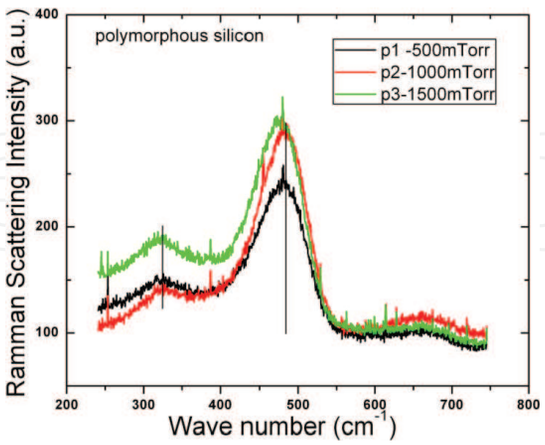

Figure 11. Raman spectra of the pm-Si:H thin films.

4.2.5. Optical properties

The optical band gap (E_{opt}) of pm-Si:H films was calculated from transmittance measurements and the method of Tauc. In **Figure 12** the Tauc plots of pm-Si:H films are shown, where the E_{opt} values were extracted. In **Table 4** the E_{opt} values are shown, and it is observed that with an increase of deposition pressure, E_{opt} has a decrement, from 1.93 eV to 1.84 eV. The obtained values in the pm-Si:H series for E_{opt} are in agreement for intrinsic pm-Si:H films which have a direct E_{opt} in the range of 1.6–1.8 eV and very large activation energy (E_a = 1 eV), when they are deposited by PECVD [35–37].

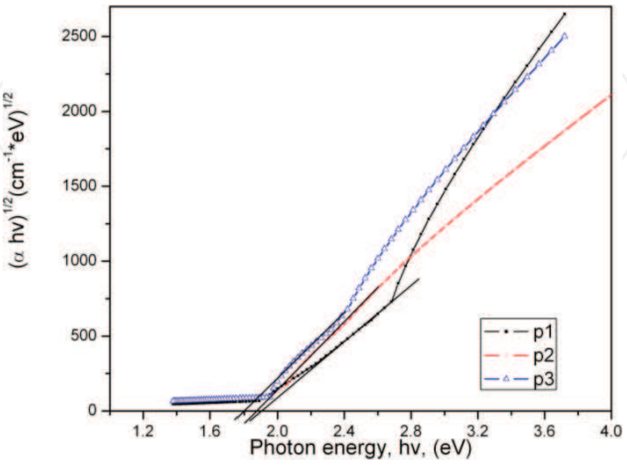

Figure 12. Optical band gap determination from the Tauc plots ($(\alpha h\nu)^{1/2}$ vs. photon energy) for pm-Si:H films as a function of the deposition pressure.

4.2.6. Electrical properties

Temperature dependence of conductivity (σ(T)) measurements were performed in the pm-Si:H films; from that characterization, the activation energy E_a was extracted; those values are shown in **Table 4**, where it is observed that the E_a values are in the range of 0.72–0.94 eV, which is in agreement with those values reported in literature [34].

As well the dark room temperature conductivity (σ_{dark}) and the photoconductivity (σ_{photo}) under AM 1.5 illumination conditions were measured in the pm-Si:H films. Notice that in the films deposited at larger deposition pressure, the σ_{dark} tends to increase as well (**Table 4**). The larger increment of σ from dark to AM 1.5 illumination in the pm-Si:H films is close to six orders of magnitude, measured in the film deposited at 1500 mTorr, which is a very interesting result for thin-film solar cells.

Sample #	Press. (mTorr)	V_d (A/s)	E_{opt} (eV)	σ_{dark} $(\Omega\text{-cm})^{-1}$	σ_{ph} $(\Omega\text{-cm})^{-1}$	E_a (eV)
P1	500	0.55	1.93	damaged	damaged	damaged
P2	1000	0.7	1.88	6.23E−9	1.04E−5	0.72
P3	1500	2.4	1.84	1.39E−9	1.01E−3	0.94

Table 4. Characteristics of pm-Si:H films deposited.

5. Microcrystalline silicon (μc-Si:H)

μc-Si:H is a silicon-based thin film, with crystals in the range of 20–700 nm [38]. Those crystals are of different orientations and grown in columns which are separated by an amorphous phase. Usually μc-Si:H films are grown from SiH_4 and H_2 gas mixtures, but also SiF_4, H_2, and Ar mixtures have been used [39]. The main parameters to grow μc-Si:H films are high H_2 dilution, moderated RF power, and high deposition pressure; according to the optimization of these parameters, the crystalline fraction can increase (Xc) and also its performance characteristics can be optimized.

In the last years μc-Si:H has gained attention due to its properties which are similar than those of polycrystalline silicon deposited by the low-pressure CVD (LPCVD). Polycrystalline silicon has a very large carriers' mobility and high stability, which make it very suitable for TFTs; however high deposition temperatures are needed (400–600°C), which limits its use in flexible substrates and even on glasses. On the other hand, μc-Si:H is deposited at low temperatures (200°C) and also exhibits high carriers' mobility, high stability, and high conductivity.

For thin-film solar cell applications, μc-Si:H also has been extensively studied due to its larger IR absorption than that of a-Si:H [39] and also larger stability against sun radiation (light soaking). At the present time, a-Si:H/μc-Si:H tandem solar cells (micromorph solar cells) have been developed with stabilized efficiencies up to 12% [9].

http://dx.doi.org/10.5772/63522

5.1. Deposition conditions of μc-Si:H

We performed a study for the production of μc-Si:H thin films in a PECVD reactor. The main parameters for the production of μc-Si:H are high pressure, moderated power, and high H_2 dilution. A series of μc-Si:H was deposited by PECVD at RF = 13.56 MHz, from a SiH_4 and H_2 and Ar mixture. **Table 5** shows the deposition conditions for the μc-Si:H thin films; those films were deposited for 30 min at substrate temperature T_s = 200°C. For the growth of the μc-Si:H films, Ar dilution has been used and the effect of the variation of the RF power density has been studied. Notice that here we present selected processes, which are more representatives.

Sample #	Pressure (mTorr)	Power (W)	Power density (mW/cm^2)	SiH_4 flow (sccm)	H_2 flow (sccm)	Ar flow
M6	1500	25	83	10	41	Yes
M7	1500	30	103	10	41	Yes
M8	1500	35	121	10	41	Yes

Table 5. Deposition conditions of μc-Si:H films.

5.2. Characterization of μc-Si:H

5.2.1. Deposition rate

The deposition rate (V_d) of the μc-Si:H films was calculated from the average thickness and the deposition time; notice that all the films were deposited for 30 min. **Figure 13** shows V_d as a function of the RF power used for the deposition of the films.

In literature it has been found that the transition from amorphous to μc-Si:H, using SiH_4 and Ar mixtures, is produced by an increment of the RF power density [37, 40]. In **Figure 13** is observed that the deposition rate decreases as the RF power increases, from 1 Å/s to 0.8 Å/s; however those values of V_d are closed to those of the films reported in literature [37, 41].

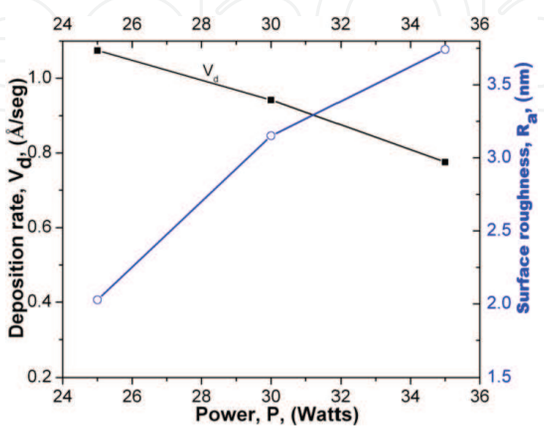

Figure 13. Deposition rate and surface roughness of μm-Si:H films as a function of the deposition pressure.

5.2.2. Structural analysis

Figures 14 (a)–(c) shows 3D AFM surface images of μc-Si:H films. In the μc-Si:H films where the RF power density was varied, we found that the film deposited at largest RF power (35 W) had the largest R_a value. The values of R_a for the μc-Si:H films are in the range of 1.9–2.5 nm (**Table 6**). Larger RF power used in the film deposition resulted in an increment of the film surface roughness, which is in agreement with [42], since larger R_a is observed in films with larger crystalline fraction [35].

Figure 15 shows a top image of a μc-Si:H thin film obtained by ultrahigh-resolution field emission scanning electron microscope (FEI Scios Dual Beam); in the figure grains of diameters of about 50 nm are observed at the surface of the μc-Si:H thin film. The surface structure is in agreement with those results observed by AFM.

Despite AFM is used to correlate the presence of silicon clusters in the film surface with the presence of silicon nanocrystals in the bulk of the film, by itself this technique is not sufficient to determine the structural composition in the bulk of the film.

HRTEM and Raman spectroscopy are techniques more suitable to determine the microcrystalline nature of the films. Figures 16 and **17** show a HRTEM transversal view of a μc-Si:H film (obtained with a FEI HRTEM Thalos F200X). In **Figure 16** crystals with different orientations can be observed, while in **Figure 17**, an amplified image is shown, where the atomic order in crystals of different orientations is observed.

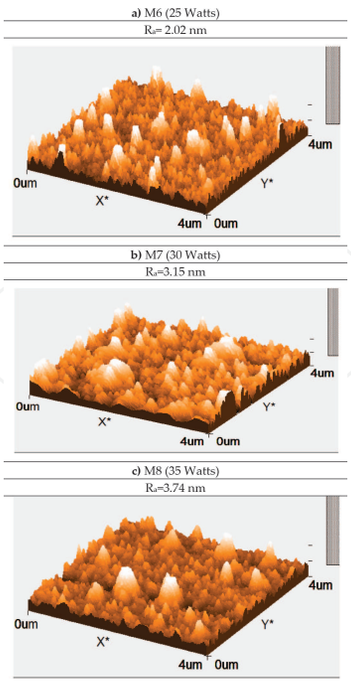

Figure 14. AFM three-dimensional images of μc-Si:H films as a function of the RF power: (a) M6 (25 W); R_a = 2.02 nm. (b) M7 (30 W); R_a = 3.15 nm. (c) M8 (35 W); R_a = 3.74 nm.

http://dx.doi.org/10.5772/63522

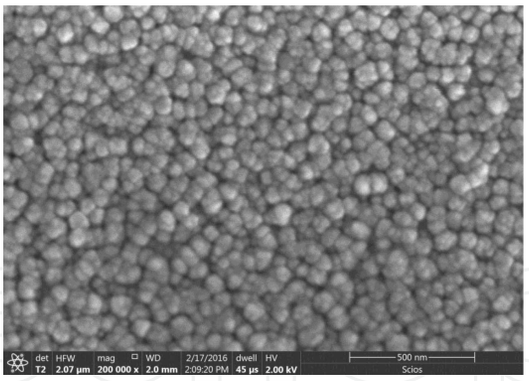

Figure 15. FE-SEM top view image of a μc-Si:H film.

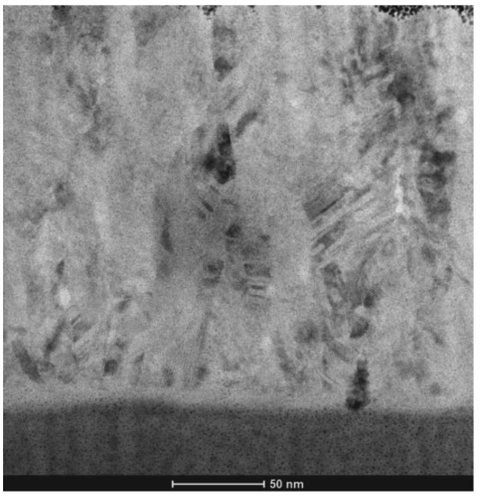

Figure 16. HRTEM transversal view of a μc-Si:H film.

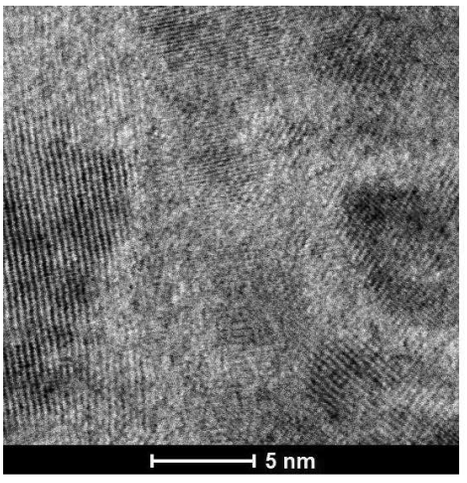

Figure 17. HRTEM transversal view of a μc-Si:H film.

5.2.3. Fourier transform infrared spectroscopy (FTIR) analysis

The IR absorbance spectra of the μc-Si:H thin films in the range 500–2200 cm^{-1} are shown in **Figure 18**. The total H_2 bonded content C_H of the films was calculated with the integration of the area under the Si—H mode (at 640 cm^{-1}) using Eq. (2), as in Section 4.2.3.

In **Figure 18**, the Si—H bonds in wagging and stretching modes are presented at 640 cm^{-1}, 700 cm^{-1}, 850 cm^{-1}, 920 cm^{-1}, and 2150 cm^{-1}, which are typical for μc-Si:H [29]. The band at 850–950 cm^{-1} observed in the samples corresponds to SiH_n bending modes; for this region low intensity is observed for the samples M7 and M8, which were deposited with larger RF power density (compared with the sample M6).

The band at 2000–2200 cm^{-1} is attributed to SiH, SiH_2, and SiH_3 stretching modes; the bands in this region are related to the presence of nanocrystals embedded in the a-Si:H matrix [41]. In **Table 6**, it is observed that the calculated H_2 content for the films of series #2 is in the range of 3–4.4%, which is low in comparison with similar work reported in literature [31]. The low H_2 content could be related to the fact that the excited Ar ion species that transfer their energy to the growing film and break the weak Si—Si bonds produced more ordered and relaxed network. In addition, large RF power density enhances the dissociation and ionization of precursor gases [35].

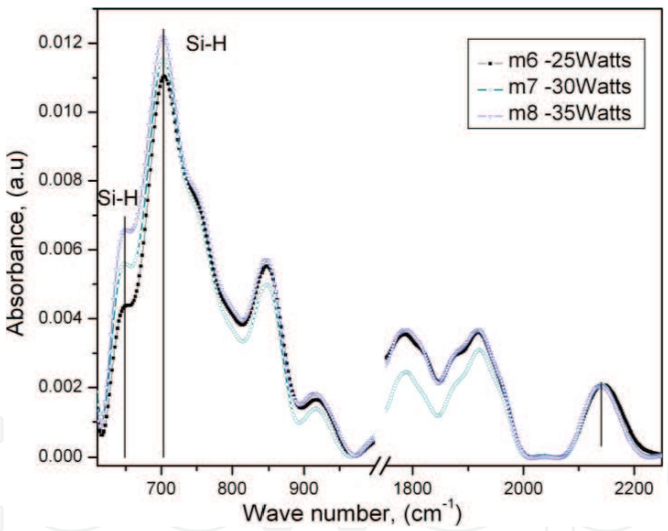

Figure 18. FTIR spectra for the μc-Si:H thin films.

Sample #	R_a (nm)	C_H (%)	$X_{C\_(Raman)}$ (%)
M6	2.02	2.9	67.9
M7	3.15	4.3	39.0
M8	3.74	4.4	55.8

Table 6. Surface roughness (R_a), H_2 content, and crystalline volume fraction for the deposited films.

http://dx.doi.org/10.5772/63522

5.2.4. Raman analysis

In **Figure 19** the Raman spectra of microcrystalline films with the presence of a peak related to a crystalline volume content are shown. The crystallinity in the samples M6–M8 is dominated by the peak at 520 cm^{-1} related to the transverse-optic (TO) mode, which is also observed for crystalline silicon [43].

In **Figure 19** an extra curve was introduced, deposited with the same deposition conditions of sample M6 but without Ar dilution, in order to observe the effect of Ar in the growth of μc-Si:H films. As is observed in **Figure 19**, that sample does not show the peak at 520 cm^{-1}, showing the importance of Ar in the dissociation of the SiH_4 molecules due to a larger ionization. In order to estimate the crystalline volume fraction ($X_{C(Raman)}$) of the films, a deconvolution in Raman peak intensities was performed using Eq. (3).

$$X_{C(Raman)} = \frac{I_c + I_m}{I_c + I_m + I_a} \tag{3}$$

where I_c is related to crystalline component at 520 cm^{-1}, I_m intermediate nanocrystalline component at 500–510 cm^{-1}, and I_a the amorphous phase at 480 cm^{-1} [43]. In **Table 6** the values of $X_{C\ (Raman)}$ obtained in the μc-Si:H films are shown.

As one can see in **Table 6**, there is no a lineal relation of X_C with respect to the increment of RF power density; the highest crystalline fraction in μc-Si:H films was found at RF power of 25 W. It is known that H_2 is present in Si—H bonds in a-Si:H deposited at low RF power and also that the H_2 content increases by increasing the RF power; in our films this behavior is presented. Therefore there is a compromise that suggests a suitable quantity of H_2 to grow μc-Si:H and a moderated RF power.

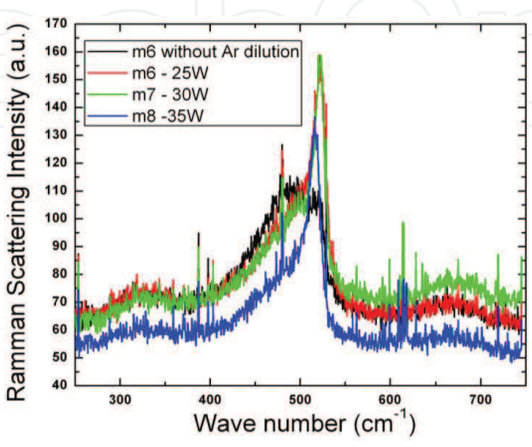

Figure 19. Raman spectra for the μc-Si:H thin films.

5.2.5. Optical properties

The optical band gap (E_{opt}) of the μc-Si:H films was calculated from transmittance measurements and the Tauc plot method. **Figure 20** shows the Tauc plots of the μc-Si:H thin films, where the RF power density was varied. For this set of samples, E_{opt} has no significant change. However the values of E_{opt} are in agreement with those reported in [33], where the μc-Si:H thin films have larger E_{opt} values than those of a-Si:H.

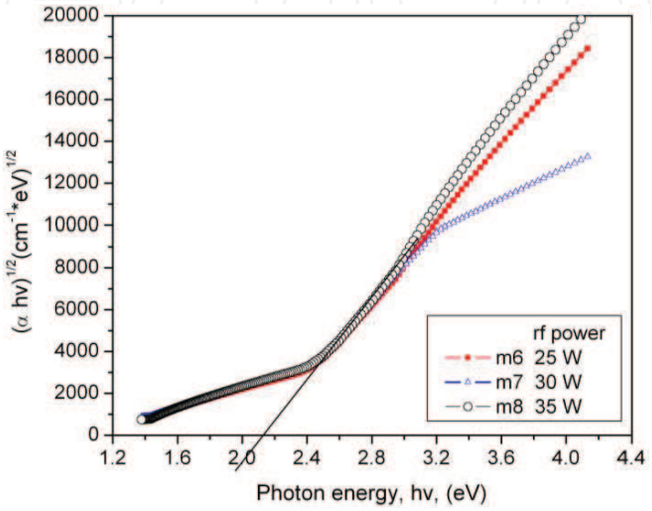

Figure 20. Optical band gap determination from the Tauc plots ($(\alpha h\nu)^{1/2}$ vs. photon energy) of μc-Si:H films as a function of the RF power.

5.2.6. Electrical properties

Temperature dependence of conductivity (σ(T)) measurements was performed in the μc-Si:H films; from that characterization the activation energy E_a was extracted, those values are shown in **Table 7**, and the E_a values are in the range of 0.15–0.27 eV, indicating doping, possibly related to oxygen contamination during deposition. Notice that the E_a values increase with an increment in the RF power.

As well the dark room temperature conductivity (σ_{dark}) and the photoconductivity (σ_{photo}) under AM 1.5 illumination conditions were measured, in the μc-Si:H films. The larger increment of σ from dark to AM 1.5 illumination in the μc-Si:H films is of about two orders of magnitude, measured in the film deposited with a RF power of 30 W (**Table 7**).

Sample #	Power (W)	V_d (A/s)	E_{opt} (eV)	σ_{dark} (Ω-cm)$^{-1}$	σ_{ph} (Ω-cm)$^{-1}$	E_a (eV)
M6	25	1.1	2.09	6.32E−7	1.21E−5	0.15
M7	30	0.9	2.1	1.59E−6	1.05E−4	0.15
M8	35	0.8	2.1	5.35E−6	7.98E−5	0.27

Table 7. Characteristics of μc-Si:H films.

http://dx.doi.org/10.5772/63522

Acknowledgements

We acknowledge to Fernando Mendoza, Diego García, and Daniel Phifer, from FEI, for their samples' preparation and HRTEM observation of the μc-Si:H films.

Author details

Mario Moreno[1*], Roberto Ambrosio[2], Arturo Torres[1], Alfonso Torres[1], Pedro Rosales[1], Adrián Itzmoyotl[1] and Miguel Domínguez[3]

*Address all correspondence to: mmoreno@inaoep.mx

1 National Institute of Astrophysics, Optics and Electronics, INAOE, Electronics Department, Puebla, Mexico

2 Electronics School, Meritorious Autonomous University of Puebla, BUAP, Puebla, Mexico

3 Research Center of Semiconductor Devices, Meritorious Autonomous University of Puebla, BUAP, Puebla, Mexico

References

[1] Roca i Cabarrocas P., Plasma enhanced chemical vapour deposition of amorphous polymorphous and microcrystalline silicon films, J. Non Cryst. Solids, 266–269, (2000) 31–37. doi: 10.1016/S0022-3093(99)00714-0.

[2] Bronner W., Kleider J.P., Bruggemann R., Mencaraglia D., Mehring M., Comparison of transport and defects properties in hydrogenated polymorphous and amorphous silicon, J. Non Cryst. Solids, 299–302, (2002) 551–555. doi: 10.1016/S0022-3093(01)01201-7.

[3] Roca i Cabarrocas P., Fontcuberta i Morral A., Lebib S., Poissant Y., Plasma production of nanocrystalline silicon thin films for large area electronic and devices, Pure Appl. Chemicals, 74 (3), (2002) 359–367. http://dx.doi.org/10.1351/pac200274030359.

[4] Brinza M., Adriaenssens G.J., Abramov A., Roca i Cabarrocas P., Influence of deposition parameters on hole mobility in polymorphous silicon, Thin Solid Films 515 (2007) 7504–7507. doi: 10.1016/j.tsf.2006.12.009

[5] Roca i Cabarrocas P., Fontcuberta i Morral A., Poissant Y., Growth and optoelectronic properties of polymorphous silicon thin films, Thin Solid Films, 403–404 (2002) 39–46. doi: 10.1016/S0040-6090(01)01656-X

[6] Fontcuberta i Morral A., Brenot R., Hamers E.A.G., Vanderhaghen R., Insitu investigation of polymorphous silicon deposition, J. Non Cryst. Solids 266–269 (2000) 48–53. doi: 10.1016/S0022-3093(99)00723-1

[7] Staebler D.L., Wronski C.R., Reversible conductivity changes in discharge-produced amorphous Si, Appl. Phys. Lett.31, 292–294 (1977). doi: 10.1063/1.89674

[8] Kim K.-H., Johnson E.V., Roca i Cabarrocas P., Irreversible light-induced degradation and stabilization of hydrogenated polymorphous silicon solar cells, Sol. Energy Mater. Sol. Cells, 105 (2012) 208–212. doi: 10.1016/j.solmat.2012.06.026.

[9] Cashmore J.S., Apolloni M., Braga A., Caglar O., Cervetto V., Fenner Y., Goldbach-Aschemann S., Goury C., Hötzel J.E., Iwahashi T., Kalas J., Kitamura M., Klindworth M., Kupich M., Leu G.-F., Lin J., Lindic M.-H., Losio P.A., Mates T., Matsunaga D., Mereu B., Nguyen X.-V., Psimoulis I., Ristau S., Roschek T., Salabas A., Salabas E.L., Sinicco I., Improved conversion efficiencies of thin-film silicon tandem (MICROMORPH™) photovoltaic modules, Sol. Energ. Mater. Sol. Cells, 144 (2016) 84–95. http://dx.doi.org/10.1016/j.solmat.2015.08.022.

[10] Van Sark W.G.J.H.M., Chapter 1 in thin films and nanostructures, vol. 30, In: Francombe M.H., ed., Advances in Plasma-Grown Hydrogenated Films, Academic Press, San Diego, 2002, 1–215.

[11] Bruno G., Capezzuto P., Madan A. eds., Plasma Deposition of Amorphous-based Materials. Academic Press Inc, San Diego, 1995.

[12] Cluster Tool for Prototyping [internet] 2016. Available from: http://www.mvsystem-sinc.com/products/cluster-tool-for-prototyping/ [Accessed: 2016-05-01]

[13] Takatsuka H., Noda M., Yonekura Y., Takeuchi Y., Yamauchi Y., Development of high efficiency large-area silicon thin film modules using VHF-PECVD, Sol. Energy 77, 6, (2004), 951–960. doi: 10.1016/j.solener.2004.06.007

[14] Watanabe T., Tanaka M., Azuma K., Nakatani M., Sonobe T., Shimada T., Microwave-excited plasma CVD of a-Si:H films utilizing a hydrogen plasma stream or by direct excitation of silane, Jpn. J. Appl. Phys. 26, 8, (1987) 1215. http://dx.doi.org/10.1143/JJAP.26.1215.

[15] Hayama M., Kobayashi K., Kawamoto S., Miki H., Onishi Y., Characteristics of a-Si:H films deposited by electron cyclotron resonance plasma CVD, J. Non Cryst. Solids 97–98, (1987) 273–276. doi: 10.1016/0022-3093(87)90065-2

[16] McCormick C.S., Weber C.E., Abelson J.R., Davis G.A., Weiss R.E., Aebi V., Low temperature fabrication of amorphous silicon thin film transistors by dc reactive magnetron sputtering, J. Vac. Sci. Technol. A 15, (1997) 2770. http://dx.doi.org/10.1116/1.580821.

[17] Jadkar S.R., Sali J.V., Funde A.M., Ali Bakr N., Vidyasagar P.B., Hawaldar R.R., Amalnerkar D.P., Deposition of hydrogenated amorphous silicon (a-Si:H) films by hot-

wire chemical vapor deposition (HW-CVD) method: role of substrate temperature, Sol. Energ. Mater. Sol. Cells, 91, (2007) 714–720. doi: 10.1016/j.solmat.2006.12.009.

[18] Brinza M., Adriaenssens G. J., Electronic properties of hydrogenated amorphous silicon prepared in expanding thermal plasmas, J. Optoelectron. Adv. Mater. 7, (2005) 73–81.

[19] Roca i Cabarrocas P., Fontcuberta i Morral A., Lebib S., Poissant Y., Plasma production of nanocrystalline silicon particles and polymorphous silicon thin films for large-area electronic devices, Pure Appl. Chem., 74 (2002) 359–367. doi: 10.1.1.545.1422.

[20] Thomas Zimmermann, High-rate growth of hydrogenated amorphous and microcrystalline silicon for thin-film silicon solar cells using dynamic very high frequency plasma-enhanced chemical vapor deposition, Writings of the research center of Jülich Ltd., Vol. 183, 2013.

[21] Ambrosio R., Moreno M., Torres A., Carrillo A., Vivaldo I., Cosme I., Heredia A., Deposition and characterization of amorphous silicon with embedded nanocrystals and microcrystalline silicon for thin film solar cells, J. Alloy Compd., 643, 1, (2015) S27–S32. doi: 10.1016/j.jallcom.2014.11.105.

[22] Moreno M., Torres A., Ambrosio R., Zuñiga C., Torres-Rios A., Monfil K., Rosales P., Itzmoyotl A., Study of the effect of the deposition parameters on the structural, electric and optical characteristics of polymorphous silicon films prepared by low frequency PECVD, Mater. Sci. Eng. B: Adv. 176 (2011) 1373–1377. doi: 10.1016/j.mseb.2011.01.022.

[23] Huang T.-C., Huang J.-L., ChengTim K.-T., Robust circuit design for flexible electronics, IEEE Des. Test Comput., 28, (2011) 8–15. doi: 10.1109/MDT.2011.74.

[24] Stutzmann M., Defect density in amorphous silicon, Philos. Mag. B: Phys. Condens. Matter 60, (1989) 531–546. doi: 10.1080/13642818908205926.

[25] Springer Handbook of Electronic and Photonic Materials, In: Kasap S., Capper P. eds., Springer Science+Business Media, Inc., New York, 2006.

[26] Deng X., Schiff E.A., Amorphous silicon based solar cells, In: Luque A., Hegedus S., eds., Handbook of Photovoltaic Science and Engineering, John Wiley & Sons, Chichester, 2003, 505–565.

[27] Matsumura H., Nakagome Y., Furukawa S., Conductivity and p–n type control of fluorinated amorphous silicon (a-Si:F) without incorporating hydrogen, J. Appl. Phys., 52, (1981), 291. http://dx.doi.org/10.1063/1.328491.

[28] Singh J., Shimakawa K., eds., Advances in Amorphous Semiconductors, Taylor & Francis, New York, 2003.

[29] Kroll U., Meier J., Shah A., Hydrogen in amorphous and microcrystalline silicon films prepared by hydrogen dilution, J. Appl. Phys. 80 (1996), 4971–4975. doi: 10.1063/1.363541. http://dx.doi.org/10.1063/1.363541.

[30] Lucovsky G., Vibrational spectroscopy of hydrogenated amorphous silicon alloys, Sol. Cells 2 (1980) 431.

[31] Lebib S., Roca iCabarrocas P., Structure and hydrogen bonding in plasma deposited polymorphous silicon thin films, Eur. Phys. J. Appl. Phys. 26 (2004) 17–27. http://dx.doi.org/10.1051/epjap:2004018.

[32] Guo L., Ding J., Yang J., Cheng G., Ling Z., Yuan N., Effects of high hydrogen dilution ratio on optical properties of hydrogenated nanocrystalline silicon thin films, Appl. Surf. Sci. 257 (2011) 9840–9845, doi: 10.1016/j.apsusc.2011.06.038

[33] Li W., Xia D., Wang H., Zhao X., Hydrogenated nanocrystalline silicon thinfilm prepared by RF-PECVD at high pressure. J. Non Cryst. Solids 356 (2010) 2552–2556. doi: 10.1016/j.jnoncrysol.2010.07.064

[34] Roca iCabarrocas P., Kim K.H., Cariou R., Labrune M., Johnson E.V., Moreno M., Torres Rios A., Abolmasov S., Kasoui S., Low temperature plasma synthesis of nanocrystals and their application to the growth of crystalline silicon and germanium thin films, Mater. Res. Soc. Symp. Proc. 1426 (2012). doi: 10.1557/opl.2012.1094

[35] Aguas H., Roca iCabarrocas P., Lebib S., Silva V., Fortunato E., Martins R., Polymorphous silicon deposited in large area reactor at 13 and 27 MHz, Thin Solid Films. 427 (2003) 6–10. doi: 10.1016/S0040-6090(02)01172-0.

[36] Amor S.B., Atyaoui M., Bousbih R., Ouertani R., Dimassi W., Ezzaouia H., Effect of substrate temperature on microstructure and optical properties of hydrogenated nanocrystalline Si thin films grown by plasma enhanced chemical vapor deposition, Sol. Energ. 103 (2014) 12–18. http://dx.doi.org/10.1016/j.solener.2014.06.024.

[37] Badran R.I., Al-Hazmi F.S., Al-Heniti S., Al-Ghamdi A.A., Li J., Xiong S., A study of optical properties of hydrogenated microcrystalline silicon films prepared by plasma enhanced chemical vapor deposition technique at different conditions of excited power and pressure, Vacuum 83 (2009), 1023–1030. doi: 10.1016/j.vacuum.2009.01.009.

[38] Shah A., Vallat-Sauvain E., Torres P., Meier J., Kroll U., Hof C., Droz C., Goerlitzer M., Wyrsch N., Vanecek M., Intrinsic microcrystalline silicon (mc-Si:H) deposited by VHF-GD (very high frequency-glow discharge): a new material for photovoltaics and optoelectronics, Mater. Sci. Eng. B 69–70 (2000) 219–226. doi: 10.1016/S0921-5107(99)00299-8

[39] Moreno M., Boubekri R., Roca P., Cabarrocas I., Study of the effect of different fraction of large grains μc-Si:H:F films on the infrared absorption on thin film solar cells, Sol. Energ. Mater. Sol. Cells 100 (2012) 16. doi: 10.1016/j.solmat.2011.05.030.

[40] Matsui T., Kondo M., Matsuda A., Origin of the improved performance of high-deposition-rate microcrystalline silicon solar cells by high-pressure glow discharge, Jpn. J. Appl. Phys. 42 (2003), L901–L903. http://dx.doi.org/10.1143/JJAP.42.L901.

[41] Tang Z., Wang W., Zhou B., Wang D., Peng S., He D., The influence of $H_2/(H_2 + Ar)$ ratio on microstructure and optoelectronic properties of microcrystalline silicon films

deposited by plasma-enhanced CVD, Appl. Surf. Sci. 255 (2009), 8867–8873. doi: 10.1016/j.apsusc.2009.06.074

[42] Roca iCabarrocas P., Chaabane N., Kharchenko A.V., Tchakarov S., Polymorphous silicon thin films produced in dusty plasma: applications to solar cells, Plasma Phys. Control. Fusion 46 (2004) B235–B243. doi: 10.1088/0741-3335/46/12B/020.

[43] Kaneko T., Onisawa K., Wakagi M., Kita Y., Minemura T., Crystalline fraction of microcrystalline silicon films prepared by plasma enhanced chemical vapor deposition using pulsed silane flow, Jpn. J. Appl. Phys. 32 (11A), (1993), 4907–4911. doi: http://dx.doi.org/10.1143/JJAP.32.4907.

IntechOpen